

Towards Faster Training of Global Covariance Pooling Networks by Iterative Matrix Square Root Normalization

Peihua Li, Jiangtao Xie, Qilong Wang, Zilin Gao
Dalian University of Technology
peihuali@dlut.edu.cn

Abstract

Global covariance pooling in convolutional neural networks has achieved impressive improvement over the classical first-order pooling. Recent works have shown matrix square root normalization plays a central role in achieving state-of-the-art performance. However, existing methods depend heavily on eigenvalue decomposition (EIG) or singular value decomposition (SVD), suffering from inefficient training due to limited support of EIG and SVD on GPU. Towards addressing this problem, we propose an iterative matrix square root normalization method for fast end-to-end training of covariance pooling networks. At the core of our method is a meta-layer designed with loop-embedded directed graph structure. The meta-layer consists of three consecutive nonlinear structured layers, which perform pre-normalization, coupled matrix iteration and post-compensation, respectively. Our method is much faster than EIG or SVD based ones, since it involves only matrix multiplications, suitable for parallel implementation on GPU. Moreover, the proposed network with ResNet architecture can converge in much less epochs, further accelerating network training. On large-scale ImageNet, we achieve competitive performance superior to existing covariance pooling networks. By finetuning our models pre-trained on ImageNet, we establish state-of-the-art results on three challenging fine-grained benchmarks.

1. Introduction

Deep convolutional neural networks (ConvNets) have made significant progress in the past years, achieving recognition accuracy surpassing human beings in large-scale object recognition [7]. The ConvNet models pre-trained on ImageNet [5] have been proven to benefit a multitude of other computer vision tasks, ranging from fine-grained visual categorization (FGVC) [23], object detection [26], semantic segmentation [24] to scene parsing [34], where labeled data are insufficient for training from scratch. The

common layers such as convolution, non-linear rectification, pooling and batch normalization [11] have become off-the-shelf commodities, widely supported on devices including workstations, PCs and embedded systems.

Although the architecture of ConvNet has greatly evolved in the past years, its basic layers largely keep unchanged [19]. Recently, researchers have shown increasing interests in exploring structured layers to enhance representation capability of networks [12, 23]. One particular kind of structured layer is concerned with global covariance pooling after the last convolution layer, which has shown impressive improvement over the classical first-order pooling, successfully used in FGVC [23], visual question answering [15] and video action recognition [31]. Very recent works have demonstrated that matrix square root normalization of global covariance pooling plays a key role in achieving state-of-the-art performance, either in large-scale visual recognition [20] or in challenging FGVC [22, 30].

For computing matrix square root, existing methods design meta-layers depending heavily on eigenvalue decomposition (EIG) or singular value decomposition (SVD) [20, 30, 22]. However, fast implementation of EIG or SVD on GPU is an open problem, which is limitedly supported on NVIDIA CUDA platform, significantly slower than their CPU counterparts [12, 22]. As such, existing methods opt for EIG or SVD on CPU for computing matrix square root. Nevertheless, current implementations of meta-layers depending on CPU are far from efficient. Particularly for multi-GPU configuration, such doing greatly hinders GPU concurrency and throughput, since GPUs with powerful parallel computing ability have to be interrupted, awaiting job completion on CPU with limited parallel ability.

In this paper, we make the effort towards addressing this problem. In [22], Lin and Maji adopt an iterative method to compute matrix square root, which, however, is only for fast inference of pretrained models, not for the purpose of end-to-end learning. Instead, during training they perform forward computation based on SVD and compute gradients of backward pass using SVD or by solving Lyapunov equation. Inspired by [22], we present an iterative matrix

Method	Foward Prop. (FP)	Backward Prop. (BP)	CUDA support	Scalability to multi-GPUs	Large-scale (LS) or Small-scale (SS)
MPN-COV [20]	EIG algorithm (matrix EIG)	BP of EIG (matrix product)	limited due to EIG	limited	LS only
G ² DeNet [30]	SVD algorithm (matrix SVD)	BP of SVD (matrix product)	limited due to SVD	limited	SS only
Improved B-CNN* [22]	SVD algorithm (matrix SVD)	BP of SVD (or BP by Lyapunov equ.) (matrix product or QR)	limited due to SVD or QR	limited	SS only
iSQRT-COV (ours)	Newton-Schulz Iter. (matrix product)	BP of Newton-Schulz Iter. (matrix product)	good	good	LS+SS

Table 1. Summary of differences between our iSQRT-COV and related methods. *Though [22] adopts Newton-Schulz iteration (called modified DB iteration therein) for network inference, it remains unclear how to perform end-to-end training based on the iterative method.

square root normalization method based on Newton-Schulz iteration [9], called iSQRT-COV, which enables backpropagation of classification error so that the ConvNet can be trained end-to-end. The main differences between our method and closely related works are presented in Tab. 1.

At the core of iSQRT-COV is a meta-layer with loop-embedded directed graph structure, designed for simultaneously ensuring convergence of Newton-Schulz iteration and competitive performance of covariance pooling networks. The meta-layer consists of three consecutive non-linear structured layers, performing pre-normalization, coupled matrix iteration and post-compensation, respectively. In terms of matrix backpropagation methodology [13], we derive gradients associated with these non-linear structured layers. The proposed iSQRT-COV is significantly faster than the competing methods and scalable to multiple GPUs. On large-scale ImageNet, we evaluate the proposed method with AlexNet and ResNet architectures, achieving performance matching or better than the competing methods. We apply our pre-trained models to challenging fine-grained classification, establishing state-of-the-art results.

2. Related Work

B-CNN is one of the first end-to-end covariance pooling ConvNets [23, 12]. It performs element-wise signed square root normalization for covariance matrix, achieving impressive performance in a variety of vision tasks such as FGVC, visual question answering and video action recognition. Recently, improved B-CNN [22] shows that the square root normalization of covariance matrix can further attain big improvement. For end-to-end learning, improved B-CNN depends on SVD for foward propagation, while deriving backward backpropagation in terms of SVD or Lyapunov equation. Note that improved B-CNN adopts the iterative method for computing matrix square root. However, their purpose is only for fast inference of pretrained models and it still remains unclear how to perform end-to-end training based on the iterative method.

Focusing on large-scale visual recognition, MPN-COV [20] proposes matrix power normalized covariance

method, with the power of 1/2 (i.e., matrix square root) being the best option. It achieves impressive improvement with architectures of AlexNet [18], VGG-Net [2, 27] and ResNet [8]. Matrix power normalization is shown to be consistent with shrinkage principle of robust covariance estimation, and furthermore, matrix square root is the unique solution of a robust von Neumann regularized maximum likelihood estimation. It is also shown that matrix power normalization approximately yet effectively exploits geometry of the manifold of covariance matrices, superior to matrix logarithm normalization for high-dimensional convolutional features. For efficiency, all computation of MPN-COV meta-layer is implemented with NVIDIA cuBLAS library running on GPU, except EIG which runs on CPU.

G²DeNet [30] inserts Gaussian distributions as global representations into networks for end-to-end training. Each Gaussian is identified as square root of a symmetric positive definite matrix constructed from the mean vector and covariance matrix. The matrix square root is also reported to play a central role in obtaining the competitive performance [30, Tab. 1 & Tab. 5]. FASON [4] proposes a fusion network combining the second-order and first-order information for end-to-end learning. Compact bilinear pooling (CBP) [6] makes it clear that bilinear pooling is closely related to the second-order polynomial kernel, and presents two compact representations via low-dimensional feature maps for kernel approximation. Kernel pooling [3] approximates Gaussian RBF kernel to a given order through compact explicit feature maps, which aims to characterize higher order feature interactions. Cai et al. [1] introduce a polynomial kernel based predictor to model higher-order statistics of convolutional features across multiple layers.

The factorized bilinear network (FBN) [21] models pairwise feature interaction by introducing a quadratic transformation with low rank constraint. In [36], Volterra-based convolution is proposed based on a computational model of the visual cortex for representing non-linear (second-order) information. The second-order response transform (SORT) [32] appends an element-wise product transform to linear sum of a two-branch network, which facilitates cross-branch propagation and increases network nonlinearity.

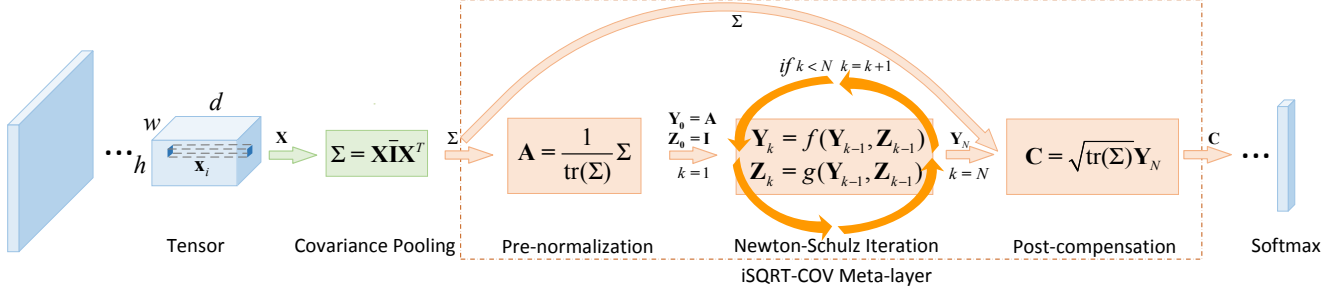


Figure 1. Proposed iterative matrix square root normalization of covariance pooling (iSQRT-COV) network. After the last convolution layer, we perform second-order pooling by estimating a covariance matrix. We design a meta-layer with loop-embedded directed graph structure for computing approximate square root of covariance matrix. The meta-layer consists of three nonlinear structured layers, performing pre-normalization, coupled Newton-Schulz iteration and post-compensation, respectively. See Sec. 3 for notations and details.

3. Proposed iSQRT-COV Network

In this section, we first give an overview of the proposed iSQRT-COV network. Then we describe matrix square root computation and its forward propagation. We finally derive the corresponding backward gradients.

3.1. Overview of Method

The flowchart of the proposed network is shown in Fig. 1. Let output of the last convolutional layer (with ReLU) be a $h \times w \times d$ tensor with spatial height h , width w and channel d . We reshape the tensor to a feature matrix \mathbf{X} consisting of $n = wh$ features of d -dimension. Then we perform second-order pooling by estimating the covariance matrix $\Sigma = \mathbf{X}\bar{\mathbf{X}}^T$, where $\bar{\mathbf{I}} = \frac{1}{n}(\mathbf{I} - \frac{1}{n}\mathbf{1})$, \mathbf{I} and $\mathbf{1}$ are the $n \times n$ identity matrix and matrix of all ones, respectively.

Our meta-layer is designed to have loop-embedded directed graph structure, consisting of three consecutive nonlinear structured layers. The purpose of the first layer (i.e., pre-normalization) is to guarantee the convergence of the following Newton-Schulz iteration, achieved by dividing the covariance matrix by its trace (or Frobenius norm). The second layer is of loop structure, repeating the coupled matrix equations involved in Newton-Schulz iteration a fixed number of times, for computing approximate matrix square root. The pre-normalization nontrivially changes data magnitudes, so we design the third layer (i.e., post-compensation) to counteract the adverse effect by multiplying trace (or Frobenius norm) of the square root of the covariance matrix. As the output of our meta-layer is a symmetric matrix, we concatenate its upper triangular entries forming an $d(d+1)/2$ -dimensional vector, submitted to the subsequent layer of the ConvNet.

3.2. Matrix Square Root and Forward Propagation

Square roots of matrices, particularly covariance matrices which are symmetric positive (semi)definite (SPD), find applications in a variety of fields including computer vision,

medical imaging [35] and chemical physics [14]. It is well-known any SPD matrix has a unique square root which can be computed accurately by EIG or SVD. Briefly, let \mathbf{A} be an SPD matrix and it has EIG $\mathbf{A} = \mathbf{U}\text{diag}(\lambda_i)\mathbf{U}^T$, where \mathbf{U} is orthogonal and $\text{diag}(\lambda_i)$ is a diagonal matrix of eigenvalues λ_i of \mathbf{A} . Then \mathbf{A} has a square root $\mathbf{Y} = \mathbf{U}\text{diag}(\lambda_i^{1/2})\mathbf{U}^T$, i.e., $\mathbf{Y}^2 = \mathbf{A}$. Unfortunately, both EIG and SVD are not well supported on GPU.

Newton-Schulz Iteration Higham [9] studied a class of methods for iteratively computing matrix square root. These methods, termed as Newton-Padé iterations, are developed based on the connection between matrix sign function and matrix square root, together with rational Padé approximation. Specifically, for computing the square root \mathbf{Y} of \mathbf{A} , given $\mathbf{Y}_0 = \mathbf{A}$ and $\mathbf{Z}_0 = \mathbf{I}$, for $k = 1, \dots, N$, the coupled iteration takes the following form [9, Chap. 6.7]:

$$\begin{aligned} \mathbf{Y}_k &= \mathbf{Y}_{k-1} p_{lm}(\mathbf{Z}_{k-1} \mathbf{Y}_{k-1}) q_{lm}(\mathbf{Z}_{k-1} \mathbf{Y}_{k-1})^{-1} \\ \mathbf{Z}_k &= p_{lm}(\mathbf{Z}_{k-1} \mathbf{Y}_{k-1}) q_{lm}(\mathbf{Z}_{k-1} \mathbf{Y}_{k-1})^{-1} \mathbf{Z}_{k-1}, \end{aligned} \quad (1)$$

where p_{lm} and q_{lm} are polynomials, and l and m are non-negative integers. Eqn. (1) converges only locally: if $\|\mathbf{A} - \mathbf{I}\| < 1$ where $\|\cdot\|$ denotes any induced (or consistent) matrix norm, \mathbf{Y}_k and \mathbf{Z}_k quadratically converge to \mathbf{Y} and \mathbf{Y}^{-1} , respectively. The family of coupled iteration is stable in that small errors in the previous iteration will not be amplified. The case of $l = 0, m = 1$ called *Newton-Schulz iteration* fits for our purpose as no GPU unfriendly matrix inverse is involved:

$$\begin{aligned} \mathbf{Y}_k &= \frac{1}{2} \mathbf{Y}_{k-1} (3\mathbf{I} - \mathbf{Z}_{k-1} \mathbf{Y}_{k-1}) \\ \mathbf{Z}_k &= \frac{1}{2} (3\mathbf{I} - \mathbf{Z}_{k-1} \mathbf{Y}_{k-1}) \mathbf{Y}_{k-1}. \end{aligned} \quad (2)$$

Clearly Eqn. (2) involves only matrix product, suitable for parallel implementation on GPU. Compared to *accurate* square root computed by EIG, one can only obtain *approximate* solution with a small number of iterations. We

determine the number of iterations N by cross-validation. Interestingly, compared to EIG or SVD based methods, experiments on large-scale ImageNet show that we can obtain matching or marginally better performance under AlexNet architecture (Sec. 4.2) and better performance under ResNet architecture (Sec. 4.3), using no more than 5 iterations.

Pre-normalization and Post-compensation As Newton-Schulz iteration only converges locally, we pre-normalize Σ by trace or Frobenius norm, i.e.,

$$\mathbf{A} = \frac{1}{\text{tr}(\Sigma)}\Sigma \text{ or } \frac{1}{\|\Sigma\|_F}\Sigma. \quad (3)$$

Let λ_i be eigenvalues of Σ , arranged in nondecreasing order. As $\text{tr}(\Sigma) = \sum_i \lambda_i$ and $\|\Sigma\|_F = \sqrt{\sum_i \lambda_i^2}$, it is easy to see that $\|\Sigma - \mathbf{I}\|_2$, which equals to the largest singular value of $\Sigma - \mathbf{I}$, is $1 - \frac{\lambda_1}{\sum_i \lambda_i}$ and $1 - \frac{\lambda_1}{\sqrt{\sum_i \lambda_i^2}}$ for the case of trace and Frobenius norm, respectively, both less than 1. Hence, the convergence condition is satisfied.

The above pre-normalization of covariance matrix non-trivially changes the data magnitudes such that it produces adverse effect on network. Hence, to counteract this change, after the Newton-Schulz iteration, we accordingly perform post-compensation, i.e.,

$$\mathbf{C} = \sqrt{\text{tr}(\Sigma)}\mathbf{Y}_N \text{ or } \mathbf{C} = \sqrt{\|\Sigma\|_F}\mathbf{Y}_N. \quad (4)$$

An alternative scheme to counterbalance the influence incurred by pre-normalization is batch normalization (BN) [11]. One may even consider without using any post-compensation. However, our experiment on ImageNet has shown that, without post-normalization, prevalent ResNet [8] fails to converge, while our scheme outperforms BN by about 1% (see 4.3 for details).

3.3. Backward Propagation (BP)

The gradients associated with the structured layers are derived using matrix backpropagation methodology [13], which establishes the chain rule of a general matrix function by first-order Taylor approximation. Below we take *pre-normalization by trace* as an example, deriving the corresponding gradients.

BP of Post-compensation Given $\frac{\partial l}{\partial \mathbf{C}}$ where l is the loss function, the chain rule is of the form $\text{tr}((\frac{\partial l}{\partial \mathbf{C}})^T d\mathbf{C}) = \text{tr}((\frac{\partial l}{\partial \mathbf{Y}_N})^T d\mathbf{Y}_N + \text{tr}((\frac{\partial l}{\partial \Sigma})^T d\Sigma)$, where $d\mathbf{C}$ denotes variation of \mathbf{C} . After some manipulations, we have

$$\begin{aligned} \frac{\partial l}{\partial \mathbf{Y}_N} &= \sqrt{\text{tr}(\Sigma)} \frac{\partial l}{\partial \mathbf{C}} \\ \frac{\partial l}{\partial \Sigma} \Big|_{\text{post}} &= \frac{1}{2\sqrt{\text{tr}(\Sigma)}} \text{tr} \left(\left(\frac{\partial l}{\partial \mathbf{C}} \right)^T \mathbf{Y}_N \right) \mathbf{I}. \end{aligned} \quad (5)$$

BP of Newton-Schulz Iteration Then we are to compute the partial derivatives of the loss function with respect to $\frac{\partial l}{\partial \mathbf{Y}_k}$ and $\frac{\partial l}{\partial \mathbf{Z}_k}$, $k = N-1, \dots, 1$, given $\frac{\partial l}{\partial \mathbf{Y}_N}$ computed by Eqn. (5) and $\frac{\partial l}{\partial \mathbf{Z}_N} = 0$. As the covariance matrix Σ is symmetric, it is easy to see from Eqn. (2) that \mathbf{Y}_k and \mathbf{Z}_k are both symmetric. According to the chain rules (omitted hereafter for simplicity) of matrix backpropagation and after some manipulations, $k = N, \dots, 2$, we can derive

$$\begin{aligned} \frac{\partial l}{\partial \mathbf{Y}_{k-1}} &= \frac{1}{2} \left(\frac{\partial l}{\partial \mathbf{Y}_k} \left(3\mathbf{I} - \mathbf{Y}_{k-1} \mathbf{Z}_{k-1} \right) - \mathbf{Z}_{k-1} \frac{\partial l}{\partial \mathbf{Z}_k} \mathbf{Z}_{k-1} \right. \\ &\quad \left. - \mathbf{Z}_{k-1} \mathbf{Y}_{k-1} \frac{\partial l}{\partial \mathbf{Y}_k} \right) \\ \frac{\partial l}{\partial \mathbf{Z}_{k-1}} &= \frac{1}{2} \left(\left(3\mathbf{I} - \mathbf{Y}_{k-1} \mathbf{Z}_{k-1} \right) \frac{\partial l}{\partial \mathbf{Z}_k} - \mathbf{Y}_{k-1} \frac{\partial l}{\partial \mathbf{Y}_k} \mathbf{Y}_{k-1} \right. \\ &\quad \left. - \frac{\partial l}{\partial \mathbf{Z}_k} \mathbf{Z}_{k-1} \mathbf{Y}_{k-1} \right). \end{aligned} \quad (6)$$

The final step of this layer is concerned with the partial derivative with respect to $\frac{\partial l}{\partial \mathbf{A}}$, which is given by

$$\frac{\partial l}{\partial \mathbf{A}} = \frac{1}{2} \left(\frac{\partial l}{\partial \mathbf{Y}_1} \left(3\mathbf{I} - \mathbf{A} \right) - \frac{\partial l}{\partial \mathbf{Z}_1} - \mathbf{A} \frac{\partial l}{\partial \mathbf{Y}_1} \right). \quad (7)$$

BP of Pre-normalization Note that here we need to combine the gradient of the loss function l with respect to Σ , backpropagated from the post-compensation layer. As such, by referring to Eqn. (3), we make similar derivations as before and obtain

$$\begin{aligned} \frac{\partial l}{\partial \Sigma} &= -\frac{1}{(\text{tr}(\Sigma))^2} \text{tr} \left(\left(\frac{\partial l}{\partial \mathbf{A}} \right)^T \Sigma \right) \mathbf{I} + \frac{1}{\text{tr}(\Sigma)} \frac{\partial l}{\partial \mathbf{A}} \\ &\quad + \frac{\partial l}{\partial \Sigma} \Big|_{\text{post}}. \end{aligned} \quad (8)$$

If we adopt *pre-normalization by Frobenius norm*, the gradients associated with post-compensation become

$$\begin{aligned} \frac{\partial l}{\partial \mathbf{Y}_N} &= \sqrt{\|\Sigma\|_F} \frac{\partial l}{\partial \mathbf{C}} \\ \frac{\partial l}{\partial \Sigma} \Big|_{\text{post}} &= \frac{1}{2\|\Sigma\|_F^{3/2}} \text{tr} \left(\left(\frac{\partial l}{\partial \mathbf{C}} \right)^T \mathbf{Y}_N \right) \Sigma \end{aligned} \quad (9)$$

and that with respect to pre-normalization is

$$\begin{aligned} \frac{\partial l}{\partial \Sigma} &= -\frac{1}{\|\Sigma\|_F^3} \text{tr} \left(\left(\frac{\partial l}{\partial \mathbf{A}} \right)^T \Sigma \right) \Sigma + \frac{1}{\|\Sigma\|_F} \frac{\partial l}{\partial \mathbf{A}} \\ &\quad + \frac{\partial l}{\partial \Sigma} \Big|_{\text{post}}, \end{aligned} \quad (10)$$

while the backward gradients of Newton-Schulz iteration (6) keep unchanged.

Finally, given $\frac{\partial l}{\partial \Sigma}$, one can derive the gradient of the loss function l with respect to input matrix \mathbf{X} , which takes the following form [20]:

$$\frac{\partial l}{\partial \mathbf{X}} = \bar{\mathbf{I}} \mathbf{X} \left(\frac{\partial l}{\partial \Sigma} + \left(\frac{\partial l}{\partial \Sigma} \right)^T \right). \quad (11)$$

4. Experiments

We evaluate the proposed method on both large-scale image classification and challenging fine-grained visual categorization tasks. We make experiments using two PCs each of which is equipped with a 4-core Intel i7-4790k@4.0GHz CPU, 32G RAM, 512GB Samsung PRO SSD and two Titan Xp GPUs. We implement our networks using MatConvNet [28] and Matlab2015b, under Ubuntu 14.04.5 LTS.

4.1. Datasets and Our Meta-layer Implementation

Datasets For large-scale image classification, we adopt *ImageNet LSVRC2012 dataset* [5] with 1,000 object categories. The dataset contains 1.28M images for training, 50K images for validation and 100K images for testing (without published labels). As in [11, 8], we report the results on the validation set. For FGVC task, we employ three popular *fine-grained benchmarks*, i.e., CUB-200-2011(Birds) [29], FGVC-aircraft (Aircrafts) [25] and Stanford cars (Cars) [17]. The Birds dataset contains 11,788 images from 200 species, with large intra-class variation but small inter-class variation. The Aircrafts dataset includes 100 aircraft classes and a total of 10,000 images with small background noise but higher inter-class similarity. The Cars dataset consists of 16,185 images from 196 classes. For all datasets, we adopt the provided training/test split, using neither bounding boxes nor annotations.

Implementation of iSQRT-COV Meta-layer We encapsulate our code in three computational blocks, which implement forward&backward computation of pre-normalization layer, Newton-Schulz iteration layer and post-compensation layer, respectively. The code is written in C++ based on NVIDIA cuBLAS on top of CUDA toolkit 8.0. In addition, we write code in C++ based on cuBLAS for computing covariance matrices. We create MEX files so that the above subroutines can be called in Matlab environment. For AlexNet, we insert our meta-layer after the last convolution layer (with ReLU), which outputs an $13 \times 13 \times 256$ tensor. For ResNet architecture, as suggested [20], we do not perform downsampling for the last set of convolutional blocks, and add one 1×1 convolution with $d = 256$ channels after the last sum layer (with ReLU). The added 1×1 convolution layer outputs an $14 \times 14 \times 256$ tensor. Hence, with both architectures, the covariance matrix Σ is of size 256×256 and our meta-layer outputs an $d(d+1)/2 = 32\text{K}$ -dimensional vector as the image representation.

4.2. Evaluation with AlexNet on ImageNet

In the first part of experiments, we analyze, with AlexNet architecture, the design choices of our iSQRT-COV method, including the number of Newton-Schulz iterations, time and memory usage, and behaviors of different

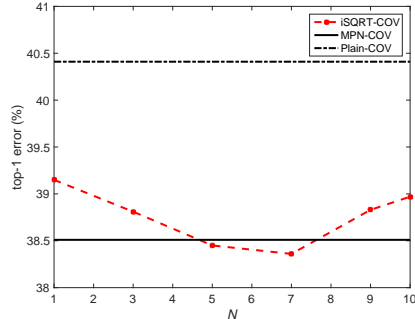


Figure 2. Impact of number N of Newton-Schulz iterations on iSQRT-COV with AlexNet architecture on ImageNet.

pre-normalization methods. We select AlexNet because it runs faster with shallower depth, and the results can extrapolate to deeper networks which mostly follow its architecture design.

We follow [20] for color augmentation and weight initialization, adopting BN and no dropout. We use SGD with a mini-batch of 128, unless otherwise stated. The momentum is 0.9 and weight decay is 0.0005. We train iSQRT-COV networks from scratch in 20 epochs where learning rate follows exponential decay $10^{-1.1} \rightarrow 10^{-5}$. All training and test images are uniformly resized with shorter sides of 256. During training we randomly crop a 224×224 patch from each image or its horizontal flip. We make inference on one single 224×224 center crop from a test image.

Impact of Number N of Newton-Schulz Iterations

Fig. 2 shows top-1 error rate as a function of number of Newton-Schulz iterations (2). Plain-COV indicates simple covariance pooling without any normalization. With one single iteration, our method outperforms Plain-COV by 1.3%. As iteration number grows, the error rate of iSQRT-COV gradually declines. With 3 iterations, iSQRT-COV is comparable to MPN-COV, having only 0.3% higher error rate, while performing marginally better than MPN-COV between 5 and 7 iterations. After $N = 7$, the error rate consistently increases, indicating growth of iteration number is not helpful for improving accuracy. As larger N incurs higher computational cost, to balance efficiency and accuracy, we set N to 5 in the remaining experiments. Notably, the approximate square root normalization improves a little over the accurate one obtained via EIG. This interesting problem will be discussed in Sec. 4.3, where iSQRT-COV is further evaluated on substantially deeper ResNets.

Time and Memory Analysis We compare time and memory consumed by single meta-layer of different methods. We adopt public code for MPN-COV and G²DeNet, released by the authors of [20] and [30], respectively. As [22] does not release code, we implement improved B-CNN

(a) Time (ms) taken and memory (MB) used by single meta-layer.

Method	Language	Bottleneck	Time	Memory
iSQRT-COV ($N=3$)	C++	N/A	0.81	0.627
iSQRT-COV ($N=5$)			1.41	1.129
MPN-COV [20]	C++&M	EIG	2.58	0.252
Impro. B-CNN [22]	M	SVD	7.46	0.502
G ² DeNet [30]	M	SVD	8.56	0.506

(b) Time (ms) taken by matrix decomposition (single precision arithmetic).

Algorithm	CUDA cuSOLVER	Matlab (CPU function)	Matlab (GPU function)
EIG	21.3	1.8	9.8
SVD	52.2	4.1	11.9

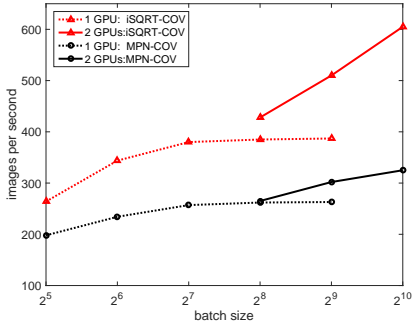
Table 2. Comparison of time and memory usage with AlexNet architecture. The size of covariance matrix is 256×256 .

Figure 3. Images per second (FP+BP) of network training with AlexNet architecture.

using Matlab Scripting language (M). As suggested [22], covariance matrices are normalized by matrix square root followed by element-wise signed square root and ℓ_2 normalization, where both FP and BP are based on SVD; Since gradient obtained by Lyapunov equation is expensive, i.e., one single call of matlab CPU routine (no GPU version) `lyap` takes 32.7ms, we do not use it for backward computation.

As shown in Tab. 2(a), iSQRT-COV ($N = 3$) and iSQRT-COV ($N = 5$) are 3.1x faster and 1.8x faster than MPN-COV, respectively. Furthermore, iSQRT-COV ($N = 5$) is 5 times more efficient than improved B-CNN and G²DeNet. Tab. 2(b) presents running time of EIG and SVD in varying implementations. Matlab built-in CPU functions and GPU functions deliver over 10x and 2.1x speedups over their CUDA counterparts, respectively. This is why MPN-COV meta-layer implements all computation on GPU except EIG which is computed by Matlab built-in CPU function. Our method needs to store \mathbf{Y}_k and \mathbf{Z}_k in Eqn. (2) which will be used in back propagation, taking up more memory than EIG or SVD based ones. Among all, our iSQRT-COV ($N = 5$) takes up the largest memory of 1.129MB, which is insignificant compared to 12GB memory on a Titan Xp. Note that for network evaluation, our method only takes 0.125MB memory as it is unnecessary to store \mathbf{Y}_k and \mathbf{Z}_k .

Method	Top-1 Error	Top-5 Error
AlexNet [18]	41.8	19.2
MPN-COV [20]	38.51	17.60
B-CNN [23]	39.89	18.32
DeepO ₂ P [12]	42.16	19.62
Improved B-CNN [22]	40.75	18.91
G ² DeNet [30]	38.71	17.66
iSQRT-COV(Frobenius)	38.78	17.67
iSQRT-COV(trace)	38.45	17.52

Table 3. Error rate (%) comparison of different covariance pooling methods with AlexNet on ImageNet.

Nowadays, multi-GPU configurations are more commonly used. They can provide larger memory and computing power, and thus can potentially accelerate training process. As such, we measure speed (images per second) of network training with two-GPU configuration. Fig. 3 presents the comparison results. For one single GPU, the speed gap vs. batch size between the two methods keeps nearly constant. For the case of two GPUs, their speed gap becomes more significant when the batch size gets larger. The speed of iSQRT-COV network continuously grows with increase of bath size while that of MPN-COV tends to saturate when batch size is larger than 512. It is not hard to account for this phenomenon. Our iSQRT-COV network runs entirely on GPUs and thus can fully exploit their computing power. In contrast, for MPN-COV network, the computation on GPUs has to be interrupted, waiting for completion of EIG on CPU and then continuing. Hence, CPU becomes a bottleneck, hindering GPU concurrency and throughput.

Pre-normalization by Trace vs. by Frobenius Norm

Sec. 3 describes two pre-normalization methods. Here we compare them in Tab. 3 (bottom rows), where iSQRT-COV (trace) indicates pre-normalization by trace. We can see that pre-normalization by trace produces 0.3% lower error rate than that by Frobenius norm. Hence, in all the remaining experiments, we adopt trace based pre-normalization method.

Comparison with Other Covariance Pooling Methods

Here we compare our iSQRT-COV with other covariance pooling methods. The results of MPN-COV, B-CNN and DeepO₂P are duplicated from [20]. Since G²DeNet and improved B-CNN do not perform large-scale classification, we train them from scratch by ourself on ImageNet. As seen in Tab. 3, our iSQRT-COV using pre-normalization by trace is marginally better than MPN-COV. All square root normalization methods except improved B-CNN outperform B-CNN and DeepO₂P. The reason that improved B-CNN performs unsatisfactorily may be that matrix power normalization followed by element-wise signed normalization does not fit for large-scale classification on ImageNet.

Pre-normalization	Post-compensation	Top-1 Err.	Top-5 Err.
Trace	w/o	N/A	N/A
	w/ BN [11]	23.12	6.60
	w/ Trace	22.14	6.22

Table 4. Impact of post-compensation on iSQRT-COV with ResNet50 architecture on ImageNet.

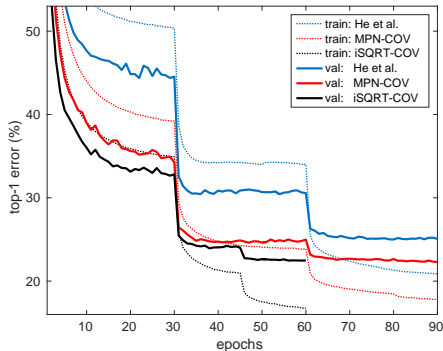


Figure 4. Convergence curves of different networks trained with ResNet50 architecture on ImageNet.

4.3. Results on ImageNet with ResNet Architecture

This section evaluates the proposed iSQRT-COV with prevalent ResNet architecture [8]. We follow [20] for color augmentation and weight initialization. We rescale each training image with its shorter side randomly sampled on [256, 512] [27]. The fixed-size 224×224 patch is randomly cropped from the rescaled image or its horizontal flip. We rescale each test image with a short side of 256 and evaluate a single 224×224 center crop for inference. We use SGD with a mini-batch size of 256, a weight decay of 0.0001 and a momentum of 0.9. We train iSQRT-COV networks from scratch up to 60 epochs, and the learning rate is initialized to $10^{-1.1}$, divided by 10 at epoch 30 and 45, respectively.

Necessity of Post-Compensation In Sec. 3, we introduce a post-compensation layer to counterbalance the adverse influence of pre-normalization which nontrivially changes data magnitudes. Rather than our scheme, one may choose Batch Normalization (BN) [11] or simply do nothing (i.e., without post-compensation). Tab. 4 summarizes impact of different schemes on iSQRT-COV network with ResNet50 architecture. Without post-compensation, iSQRT-COV network fails to converge. Careful observations show that in this case the gradients are very small (on the order of 10^{-5}), and largely tuning of learning rate helps little. Option of BN helps the network converge, but producing about 1% higher error rate than our scheme. The comparison above suggests the necessity of our post-compensation scheme.

Fast Convergence of iSQRT-COV Network We compare convergence of iSQRT-COV and MPN-COV with

Method	Model	Top-1 Err.	Top-5 Err.
He et al. [8]	ResNet50	24.7	7.8
FBN [21]		24.0	7.1
SORT [32]		23.82	6.72
MPN-COV [20]		22.73	6.54
iSQRT-COV		22.14	6.22
He et al. [8]	ResNet101	23.6	7.1
iSQRT-COV	ResNet101	21.21	5.68
He et al. [8]	ResNet152	23.0	6.7

Table 5. Error (%) comparison of second-order networks with first-order ones on ImageNet.

ResNet50 architecture, as well as the original ResNet50 of He et al. [8], which performs global average pooling after the last convolution layer. Fig. 4 presents the convergence curves. Compared to the original ResNet50, the convergence of both iSQRT-COV and MPN-COV is significantly faster. We can also see iSQRT-COV converges more rapidly than MPN-COV; within 60 epochs it achieves top-1 error 22.14%, $\sim 0.6\%$ lower than MPN-COV. The fast convergence property of iSQRT-COV is appealing. As far as we know, previous networks with ResNet50 architecture require at least 90 epochs to converge to competitive results.

Now we account for why iSQRT-COV with approximate square root normalization improves over MPN-COV performing accurate one. We conjecture there exist two reasons. First, recall that, with AlexNet architecture, the error rate curve vs. number N of Newton-Schulz Iterations (Fig. 2) indicates more accurate square root is not helpful for achieving the best result. That fact, together with fast convergence of substantially deeper ResNet50 (Fig. 4), suggests that accurate square root is not necessarily the best option, and instead, the approximate one may be more suitable. Second, the pre-normalization, designed originally for guaranteeing the convergence of Newton-Schulz iteration, may be numerically beneficial for the network convergence. Despite the above analysis, this issue is worth further research.

Comparison with State-of-the-arts In Tab. 5, we compare our method with other second-order networks, as well as the original ResNets. With ResNet50 architecture, all the second-order networks improve over the first-order one while our method performing best. MPN-COV and iSQRT-COV, both of which involve square root normalization, are superior to FBN which uses no normalization and SORT which introduces dot product transform in the linear sum of two-branch module. Moreover, our iSQRT-COV outperforms MPN-COV by 0.6% in top-1 error. Note that our 50-layer iSQRT-COV network achieves lower error rate than much deeper ResNet101 and ResNet152, while our 101-layer iSQRT-COV network outperforming the original ResNet101 by 2.4% and ResNet152 by 1.8%, respectively.

Method	Model	d	Dim.	Top-1 Err.	Top-5 Err.
He et al. [8]	ResNet50	N/A	2K	24.7	7.8
iSQRT-COV		64	2K	23.73	6.99
		128	8K	22.78	6.43
		256	32K	22.14	6.22

Table 6. Results of compact iSQRT-COV on ImageNet.

Compactness of iSQRT-COV As described earlier, our iSQRT-COV outputs one 32k-dimensional vector as an image representation. Here we consider to further compress this representation, using a simple scheme of decreasing number of channels d of 1×1 convolution inserted before our covariance pooling. The 1×1 convolution layer is initialized randomly, like all other convolution ones. PCA-initialization of this layer [23] is not viable since obtaining the principal components is too expensive: one has to scan the whole ImageNet for feature extraction from a pre-trained model and then compute SVD of a $2048 \times N$ matrix (N is often on the order of 10^5 or 10^6). Note that CBP [6] is not applicable to our iSQRT-COV, as it does not *explicitly* estimate the covariance matrix. Tab. 6 summarizes results of compact iSQRT-COV. The recognition error increases slightly ($\uparrow 0.64\%$) when d decreases from 256 to 128 (correspondingly, dimension (Dim.) of image representation $32K \rightarrow 8K$). The error rate is 23.73% if the dimensionality is compressed to 2K, still outperforming the original ResNet50 which performs global average pooling.

4.4. Fine-grained Visual Categorization

Finally, we apply the iSQRT-COV models pretrained on ImageNet to FGVC task. We follow [23, 22] for experimental setting and evaluation protocol. On all three datasets, we crop 448×448 patches as input images. We replace 1000-way softmax layer of a pre-trained iSQRT-COV model by a k -way softmax layer, where k is number of classes in the fine-grained dataset, and finetune the network using SGD with momentum of 0.9 for 50 – 100 epochs with a small learning rate ($lr=10^{-2.1}$) for all layers except the softmax layer, which is set to $5 \times lr$. We use horizontal flipping as data augmentation. After finetuning, the output of iSQRT-COV layer is ℓ_2 -normalized and then inputted to train k one-vs-all linear SVMs with hyperparameter $C = 1$; For inference, a test image is predicted by averaging scores of image and its horizontal flip computed from trained SVMs.

Tab. 7 presents classification results of different methods, where column 3 lists the dimension of the corresponding representation. With ResNet50 architecture, KP performs much better than CBP; our iSQRT-COV (8K) outperforms KP (14K) by about 2.6%, 3.8% and 0.6% on Birds, Aircrafts and Cars, respectively, though KP combines first-order up to fourth-order information while we only use second-order one. Our method improves further when the dimension of the representation is raised to 32K.

	Method	Dim.	Birds	Aircrafts	Cars
ResNet50	iSQRT-COV	32K	88.1	90.0	92.8
		8K	87.3	89.5	91.7
	CBP [6]	14K	81.6	81.6	88.6
	KP [3]	14K	84.7	85.7	91.1
VGG-D	CBP [6]	8K	84.3	84.1	91.2
	KP [3]	13K	86.2	86.9	92.4
	LRBP [16]	10K	84.2	87.3	90.9
	Improved B-CNN[22]	262K	85.8	88.5	92.0
	G ² DeNet [30]	263K	87.1	89.0	92.5
	HIHCA [1]	9K	85.3	88.3	91.7
iSQRT-COV with ResNet101		32K	88.7	91.4	93.3

Table 7. Comparison of accuracy (%) on fine-grained benchmarks.

Notably, on all fine-grained datasets, KP and CBP with 16-layer VGG-D perform better than their counterparts with 50-layer ResNet, despite the fact that ResNet50 outperforms VGG-D by a large margin on ImageNet [8]. The reason may be that the original ResNet50 outputs 2048-dimensional features which is so high that existing second- or higher-order methods cannot handle properly. This may also account for why state-of-the-art results are achieved using VGG-D model in which the last convolution layer outputs features of 512-dimension, much lower than 2048-dimension in ResNets. Different from existing second- or higher-order pooling methods which use the first-order pre-trained models, our pretrained models themselves are second-order, and thus we circumvent the aforementioned problem. Using pre-trained iSQRT-COV models with ResNet50 architecture, we achieve recognition results superior to all the compared methods, and furthermore, establish state-of-the-art results on three fine-grained benchmarks using iSQRT-COV model with ResNet101 architecture.

5. Conclusion

We presented a fast matrix square root normalized covariance (iSQRT-COV) pooling network which can be trained end-to-end. Compared to existing works depending heavily on GPU unfriendly EIG or SVD, our method, based on coupled Newton-Schulz iteration [9], is much faster since it involves only matrix multiplications, suitable for parallel implementation on GPU. With prevalent ResNet architecture, the proposed network shows faster convergence and higher recognition accuracy than MPN-COV [20]. We also established state-of-the-art results on three challenging fine-grained benchmarks (Birds, Aircrafts and Cars) by finetuning the iSQRT-COV models pre-trained on ImageNet. The proposed meta-layer is prefabricated, of no learning parameters and has compact representation. In future we are interested to integrate our iSQRT-COV meta-layer into other network architectures such as Inception [11], ResNeXT [33] and DenseNet [10].

References

- [1] S. Cai, W. Zuo, and L. Zhang. Higher-order integration of hierarchical convolutional activations for fine-grained visual categorization. In *ICCV*, Oct 2017. 2, 8
- [2] K. Chatfield, K. Simonyan, A. Vedaldi, and A. Zisserman. Return of the devil in the details: Delving deep into convolutional nets. In *BMVC*, 2014. 2
- [3] Y. Cui, F. Zhou, J. Wang, X. Liu, Y. Lin, and S. Belongie. Kernel pooling for convolutional neural networks. In *CVPR*, July 2017. 2, 8
- [4] X. Dai, J. Yue-Hei Ng, and L. S. Davis. FASON: First and second order information fusion network for texture recognition. In *CVPR*, July 2017. 2
- [5] J. Deng, W. Dong, R. Socher, L.-J. Li, K. Li, and L. Fei-Fei. ImageNet: A large-scale hierarchical image database. In *CVPR*, 2009. 1, 5
- [6] Y. Gao, O. Beijbom, N. Zhang, and T. Darrell. Compact bilinear pooling. In *CVPR*, June 2016. 2, 8
- [7] K. He, X. Zhang, S. Ren, and J. Sun. Delving deep into rectifiers: Surpassing human-level performance on ImageNet classification. In *ICCV*, 2015. 1
- [8] K. He, X. Zhang, S. Ren, and J. Sun. Deep residual learning for image recognition. In *CVPR*, 2016. 2, 4, 5, 7, 8
- [9] N. J. Higham. *Functions of Matrices: Theory and Computation*. SIAM, Philadelphia, PA, USA, 2008. 2, 3, 9
- [10] G. Huang, Z. Liu, L. van der Maaten, and K. Q. Weinberger. Densely connected convolutional networks. In *CVPR*, July 2017. 9
- [11] S. Ioffe and C. Szegedy. Batch normalization: Accelerating deep network training by reducing internal covariate shift. In *ICML*, 2015. 1, 4, 5, 7, 9
- [12] C. Ionescu, O. Vantzos, and C. Sminchisescu. Matrix backpropagation for deep networks with structured layers. In *ICCV*, 2015. 1, 2, 6
- [13] C. Ionescu, O. Vantzos, and C. Sminchisescu. Training deep networks with structured layers by matrix backpropagation. *arXiv*, abs/1509.07838, 2015. 2, 4
- [14] B. Jansík, S. Høst, P. Jørgensen, J. Olsen, and T. Helgaker. Linear-scaling symmetric square-root decomposition of the overlap matrix. *J. of Chemical Physics*, pages 124104–124104, 2007. 3
- [15] K. Kafle and C. Kanan. An analysis of visual question answering algorithms. In *ICCV*, Oct 2017. 1
- [16] S. Kong and C. Fowlkes. Low-rank bilinear pooling for fine-grained classification. In *CVPR*, July 2017. 8
- [17] J. Krause, M. Stark, D. Jia, and F. F. Li. 3D Object representations for fine-grained categorization. In *ICCV Workshops*, pages 554–561, 2013. 5
- [18] A. Krizhevsky, I. Sutskever, and G. E. Hinton. ImageNet classification with deep convolutional neural networks. In *NIPS*, pages 1097–1105, 2012. 2, 6
- [19] Y. Lecun, L. Bottou, Y. Bengio, and P. Haffner. Gradient-based learning applied to document recognition. *Proceedings of the IEEE*, 86(11):2278–2324, 1998. 1
- [20] P. Li, J. Xie, Q. Wang, and W. Zuo. Is second-order information helpful for large-scale visual recognition? In *ICCV*, Oct 2017. 1, 2, 5, 6, 7, 9
- [21] Y. Li, N. Wang, J. Liu, and X. Hou. Factorized bilinear models for image recognition. In *ICCV*, 2017. 2, 7
- [22] T.-Y. Lin and S. Maji. Improved bilinear pooling with CNNs. In *BMVC*, 2017. 1, 2, 6, 8
- [23] T.-Y. Lin, A. RoyChowdhury, and S. Maji. Bilinear CNN models for fine-grained visual recognition. In *ICCV*, 2015. 1, 2, 6, 8
- [24] J. Long, E. Shelhamer, and T. Darrell. Fully convolutional networks for semantic segmentation. In *CVPR*, June 2015. 1
- [25] S. Maji, E. Rahtu, J. Kannala, M. Blaschko, and A. Vedaldi. Fine-grained visual classification of aircraft. *HAL - INRIA*, 2013. 5
- [26] J. Redmon and A. Farhadi. YOLO9000: Better, faster, stronger. In *CVPR*, July 2017. 1
- [27] K. Simonyan and A. Zisserman. Very deep convolutional networks for large-scale image recognition. In *ICLR*, 2015. 2, 7
- [28] A. Vedaldi and K. Lenc. MatConvNet – convolutional neural networks for MATLAB. In *ACM on Multimedia*, 2015. 5
- [29] C. Wah, S. Branson, P. Welinder, P. Perona, and S. Belongie. The Caltech-UCSD Birds200-2011 Dataset. *California Institute of Technology*, 2011. 5
- [30] Q. Wang, P. Li, and L. Zhang. G2DeNet: Global Gaussian distribution embedding network and its application to visual recognition. In *CVPR*, July 2017. 1, 2, 6, 8
- [31] Y. Wang, M. Long, J. Wang, and P. S. Yu. Spatiotemporal pyramid network for video action recognition. In *CVPR*, July 2017. 1
- [32] Y. Wang, L. Xie, C. Liu, S. Qiao, Y. Zhang, W. Zhang, Q. Tian, and A. Yuille. SORT: Second-order response transform for visual recognition. In *ICCV*, 2017. 2, 7
- [33] S. Xie, R. Girshick, P. Dollar, Z. Tu, and K. He. Aggregated residual transformations for deep neural networks. In *CVPR*, July 2017. 9
- [34] B. Zhou, H. Zhao, X. Puig, S. Fidler, A. Barriuso, and A. Torralba. Scene parsing through ADE20K dataset. In *CVPR*, 2017. 1
- [35] D. Zhou, I. L. Dryden, A. A. Koloydenko, K. M. Audenaert, and L. Bai. Regularisation, interpolation and visualisation of diffusion tensor images using non-Euclidean statistics. *Journal of Applied Statistics*, 43(5):943–978, 2016. 3
- [36] G. Zoumpourlis, A. Doumanoglou, N. Vretos, and P. Daras. Non-linear convolution filters for CNN-based learning. In *ICCV*, 2017. 2